MDPI

Article

A non-inductive magnetic eye-tracker: from dipole tracking to gaze retrieval.

Valerio Biancalana [1,*] ⓘ **, Piero Chessa** [2] ⓘ,

[1]   DSFTA, University of Siena, Via Roma 56, 53100 Siena, Italy

[2]   Dept. of Physics "E.Fermi", University of Pisa, Largo Pontecorvo 3, 56127 Pisa, Italy

*   Correspondence: valerio.biancalana@unisi.it

1   **Abstract:** An innovative wearable eye tracker based on a permanent-magnet marked corneal lens
2   is analyzed in terms of the information that can be retrieved from the tracking parameters. We
3   demonstrate that, despite missing information due to the axial symmetry of the measured field,
4   physiological constraints or measurement conditions make possible to infer complete eye-pose data.
5   The results show that the instrumentation considered is suitable as a new low-invasive medical
6   diagnostics for the characterization of ocular movement and associated disorders.

7   **Keywords:** Eye Tracking; Magnetic tracker; Magnetoresistor; Magnetic Sensor; Sensor Array;
8   Microcontroller; Eye Motion, Donders' law, Listing's law

---

1. Introduction

10   The localization of magnetostatic sources on the basis of multiple measurements performed in
11 known, pre-assigned positions is widely studied and finds application in several areas, including medical
12 diagnostics [1–3]. Setups based on permanent-magnet sources enable wireless measurements, which
13 come with low invasivity and low cost. The developed methodology produces rich tracking data that
14 include both target position and orientation and presents the advantage of an occlusion-free detection.
15 Modern highly magnetized materials and solid-state magnetometric devices help to reduce the invasivity
16 level and to improve the portability/wearability of the required instrumentation. We have recently
17 demonstrated that this methodology can achieve sufficient time and space resolution to be applicable
18 also to eye-tracking.

19   Concerning the instrumentation aimed to track ocular movements, devices with diverse degrees
20 of invasivity, accuracy, speed, wearability have been developed on the basis of several concurrent
21 technologies. The latter include electro-oculography[4], infrared-reflection devices [5,6], video cameras
22 [7,8], and inductive magnetic receivers (scleral search coil, SSC) [9–12]. In this list, the former items are
23 less precise and invasive while the latter is considered the top-performance at expenses of a noticeable
24 invasivity.

25   Our non-inductive magnetometric instrumentation for eye-tracking is characterized by an
26 intermediate level of invasivity (much less than SSC), low intrusivity (it is fully wearable), low cost (<1
27 k€), high speed (>100 Sa/s), high precision (< 1 degree) and good robustness with respect to external
28 disturbances, such as eye-blinking, facial muscles actuation and fluctuations of ambient illumination.
29 In addition, after a preliminary calibration of the sensors, it does not require additional (patient based)
30 re-calibrations.

31   Apart from some works aimed to localize multiple [13–15] or distributed [16,17] magnetic sources,
32 most of the magnetic trackers reported in the literature use some numerical algorithms to infer the
33 magnetic target pose (position and orientation) modeling the magnet in terms of a dipolar field source.
34 Our device does not make an exception to this common rule, but, differing from other setups, it tracks

both the target pose and the ambient field, making the latter no longer a disturbance term, but a source of additional information.

Like other single-target systems, our device provides comprehensive dipole pose information, which however is not sufficient to fully characterize the target object's pose, even if simply modeled as a rigid body. More explicitly, the information that can be extracted from dipole tracking includes three spatial and two angular co-ordinates (the system being blind to rotations around the dipole direction), thus only 5 out of the 6 degrees of freedom (DoF) of a free rigid body can be retrieved.

This paper provides an analysis of the information that can be retrieved from the 5 DoF data produced by a dipole tracker. We specifically address the case of a dipole eye-tracker, in which physiological constraints and/or predetermined maneuvers offer complementary information and make the tracking output data sufficient to fully determine the eye pose.

The paper is organized as follows: after a brief description of the developed instrumentation and of the tracking parameters obtained from the data analysis (Sec.2), we describe in Sec.3 several approaches that enable a complete eye-pose retrieval from the dipole pose information. In the same section some examples of the retrieved gaze trajectories are reported. In particular we discuss how the dipole-gaze misalignment may affect the estimated gaze trajectory and how physiological constraints can be taken into account to improve the accuracy. Conclusion and perspectives are drawn in Sec.4.
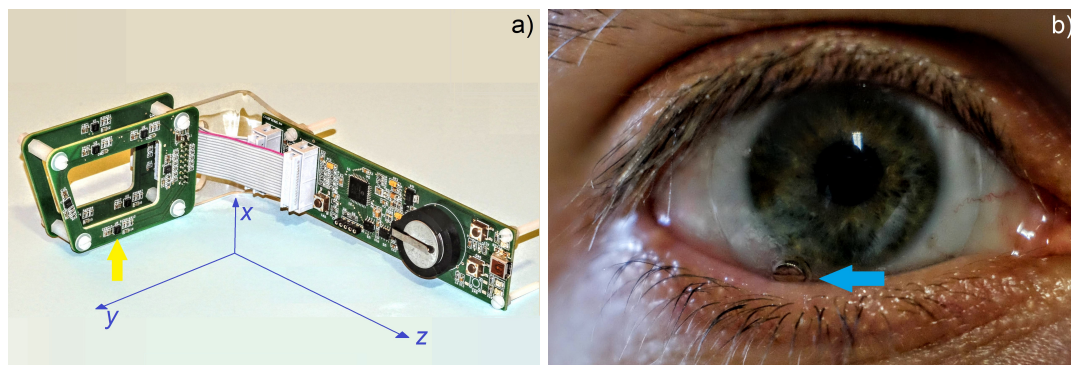
2. Setup

Figure 1. The sensor array –at the left side of image (a)– contains eight three-axial magnetoresistive sensors (one of which is indicated by the yellow arrow) distributed on two parallel printed circuit boards (PCB) displaced by $\Delta z = 16.6$ mm). A third PCB –at the right side of the image (a)– hosts a microcontroller and other electronics necessary to store data during preliminary calibration procedures and to communicate with a personal computer *via* a USB interface. The system is designed to localize a small magnet –pointed out by the blue arrow in the image (b)–, which is inserted in a scleral lens to be worn by the patient.

2.1. Sensors and hardware

The hardware of the eye tracker is shown in Fig.1 a. Its structure is extensively described in the ref. [18]. The core of the device is made of eight three-axial magnetoresistive sensors [19] that generate a total of 24 data per measurement. A microcontroller interfaces the sensors to a personal computer. The user may set sensitivity, acquisition rate and operation mode. Operation modes exist for sensors' precalibration and for tracking operation, which includes data recording and/or immediate analysis and visualization.

The sensors are included in highly integrated circuits, which also contain preconditioning electronics and analog-to-digital converters (14 bit, up to 200 Sa/s). They communicate with the microcontroller *via* eight independent I^{2}C buses, while the microcontroller is connected to PC *via* a USB interface. This architecture helps accelerate the data transfer and makes possible to acquire synchronized measurements from all the sensors.

65 The magnetoresistances have a quite linear response, but their gains may differ from the nominal
66 value causing an anisotropic response for each sensor and different responses from one sensor to the other.
67 In addition, each magnetoresistance output is affected by a non-negligible offset. Thus a pre-calibration
68 procedure is necessary, to equalize the gains and to identify and subtract the offsets [18].

69 *2.2. Data elaboration to extract tracking parameters*

70 The main scope of the described instrumentation is to retrieve the eye orientation from the pose
71 of a small magnet embedded in a scleral lens worn by the patient (Fig.1 b). The position and the
72 orientation of the target-magnet are inferred from a set of simultaneous field measurements performed
73 in pre-assigned positions. The measured field is modeled as a dipolar one generated by the magnet,
74 superposed to an external one (the Earth field), which is assumed to be homogeneous over the volume
75 occupied by the sensors.
76 The determination of the magnet pose (orientation and position) and intensity (dipole modulus),
77 plus intensity and orientation of the environmental field constitute an inverse problem, which is solved
78 by means of numeric tools.
79 The size of the magnet (0.5 mm thick and 2 mm in diameter) is selected in such a way as to make
80 its field on the sensors of the same order of magnitude as the Earth field (few tens of microtesla), which
81 creates a good condition to accurately identify both the magnet pose and the environmental field.
82 We have investigated the reliabilty of ordinary best-fitting procedures obtaining encouraging results
83 [20]. In particular, we verified that a Levenberg-Marquardt minimization algorithm is sufficiently fast
84 and adequately robust with respect to the initial guess: there exists a volume larger than zone in which
85 the magnet can move, such that if the initial guess considers the dipole in that volume with an arbitrary
86 orientation, the algorithm converges systematically to the correct solution.
Having equalized the readings to convert them in calibrated magnetometric data $\vec{B}_k^{(\text{meas})}$, solving
the inverse problem requires to minimize the quantity:

$$S = \sum_k \left| \vec{B}_k^{(\text{meas})} - B_k^{(\text{mod})} \right|^2 \tag{1}$$

being $k = 0 \dots 7$ the sensor index, and

$$\vec{B}_k^{(\text{mod})}(\vec{r}, \vec{m}) = \frac{\mu_0}{4\pi} \left(3 \frac{[\vec{m} \cdot (\vec{r}^{(k)} - \vec{r})](\vec{r}^{(k)} - \vec{r})}{\left| \vec{r}^{(k)} - \vec{r} \right|^5} - \frac{\vec{m}}{\left| \vec{r}^{(k)} - \vec{r} \right|^3} \right) + \vec{B}_{geo}, \tag{2}$$

87 the field expected on the basis of the dipole model, in the position $\vec{r}^{(k)}$ of the kth sensor, being $\vec{m}$ a
88 magnetic dipole placed in the position $\vec{r}$. The term $\vec{B}_{geo}$ accounts for the uniform environmental field.
89 The positions $\{\vec{r}^{(k)}\}$ are referred to the sensor frame, which is rigidly connected to the patient's head.
90 The best fit procedure minimizes S and outputs the estimates of $\vec{r}, \vec{m}, \vec{B}_{geo}$, for a total of nine tracking
91 parameters. As discussed in Ref.[20], under some conditions, the number of fitting parameters can
92 be reduced to eight after having determined the modulus of $\vec{m}$, while it is definitely inopportune to
93 assume a fixed value for $|\vec{B}_{geo}|$, because the environmental field is commonly enough homogeneous on
94 the volume of the array, but can vary significantly when the array is moved within the room where the
95 system operates.

96 *2.3. From tracking parameters to eye (and head) pose*

97 Once the minimization algorithm outputs the estimate of $\vec{r}, \vec{m}$ and $\vec{B}_{geo}$, the pose of eye and
98 head can be inferred. While $\vec{r}, \vec{m}$ provide information of the eye pose with respect to the sensor array,
99 the measure of the environmental field can be used as a three-dimensional compass to evaluate the
100 absolute orientation of the sensor array, i.e. of the patient's head. Combining relative eye-gaze and
101 head orientations enables the determination of the absolute gaze [21]. In addition, the comparison of
102 eye and head angular motions can be used to evaluate the eye actuation in response to head rotation,

such as in measurements of vestibulo-ocular reflex (VOR)[22] (see also Sec.3.3). However, this paper focuses on the analysis of the eye pose relative to the head, and we are not considering further the retrieval of head pose from $\vec{B}_{geo}$.

The orientation of $\vec{m}$ is related to eye rotations, but it does not provide the gaze direction directly, unless the magnetic dipole is parallel to the optical axis of the eye (let the latter be $\hat{e}$). Eye rotations around the $\vec{m}$ direction would not be revealed. This has a twofold consequence: if $\vec{m} \parallel \hat{e}$, torsional angular displacements are not detected; if $\vec{m} \nparallel \hat{e}$, some *extra assumptions* are necessary to infer $\hat{e}$ from $\vec{m}$, and, in particular, rotations around $\vec{m}$ would affect $\hat{e}$ without being detected.

It is worth recalling that besides $\vec{m}$, the best-fit procedure outputs the magnet position $\vec{r}$, which provides additional information about eye motion. However, the position co-ordinates are known with respect to the sensor reference frame and not to the eye center, thus the eye gaze cannot be retrieved directly from $\vec{r}$. Despite this feature, the partially redundant information given by $\vec{r}$ could be used in conjunction with that extracted from $\vec{m}$ to improve or to complete the eye pose reconstruction, as it will be discussed in Sec.3.6.

3. Gaze retrieval

In this section we examine procedures that can be followed to retrieve the eye gaze with respect to the sensor frame from the tracker output, more specifically from the estimates of $\vec{m}$ and $\vec{r}$. Eye translations, that can in principle be studied with an adequate analysis of $\vec{r}$ will not be taken into consideration, and we will focus on eye-ball rotations, modelling the eye as a rigid sphere rotating about its (fixed) center. Although mathematically unnecessary, this will turn in a useful simplification of the following $\vec{m}$-related discussion with no further hypothesis or loss of information. Besides, the fixed-center rigid sphere model applies to the $\vec{r}$ information discussion in the realistic approximation of very small displacements of the eye-ball center compared to the eye radius.

It has to be pointed out that the pose of a rigid body freely rotating about an assigned point requires three angular parameters to be fully defined. In other terms, generally speaking, the faced problem has 3 degrees of freedom (DoF). The modulus of the magnetic dipole is nominally constant, and the tracking uses its direction $\hat{m}$ only, thus the analysis of the unitary vector $\hat{m}$ provides only bidimensional information, e.g. the zenithal and azimutal angles, when described in spherical co-ordinates. These 2D data are not sufficient to determine the 3 DoF orientation of the eye-ball: it is necessary to consider reduced-DoF problems to achieve complete pose determination.

3.1. Small-angle and near-front sight approximation

A simple case is obtained in the hypothesis that torsional movements can be neglected and that the angle between the gaze and the front direction ($\hat{z}$ in the notation of our setup, see Fig.1) is maintained small.

In this hypothesis the current gaze $\hat{e}_k$ is always nearly parallel to $\hat{z}$ and it can be expressed as $\hat{e}_k = R\,\hat{e}_0$, being

$$R = \begin{pmatrix} 1 & 0 & \phi_y \\ 0 & 1 & \phi_x \\ -\phi_y & -\phi_x & 1 \end{pmatrix} \tag{3}$$

the first-order approximation of a rotation matrix whose parameters ϕ_x, ϕ_y represent small rotation angles around the x and the y axes respectively. The same rotation applies to the magnetic moment $\vec{m}_0$, as it is rigidly connected to the eye-ball. Thus $\hat{m}_k = R\,\hat{m}_0$, and the two angles ϕ_x, ϕ_y can be retrieved from this last relation.

Here $\hat{e}_0$ is the front sight gaze, $\hat{m}_0$ is the corresponding orientation of the dipole, and $\hat{e}_k$ is the gaze at the kth measurement, to be inferred from the estimated dipole $\vec{m}_k$. In this approach, $\hat{e}_0$ is assumed to coincide with $\hat{z}$, and $\hat{m}_0$ should be known from an independent characterization of the magnet in the scleral lens, or tentatively assigned as it will be explained below.

3.2. Larger rotations about the front ($\hat{z}$) direction

A more complex case occurs when the first-order approximation is not applicable. If so, even with the simplifying hypothesis $\hat{e}_0 \parallel \hat{z}$, the eyeball rotation cannot be, in general, resolved as a sequence of two rotations around arbitrary axes. As we will see in the following, further information is needed in this case, like a known rotation axis or a model for the eye movements. As an intuitive proof of this, consider the two-angle rotations around the pre-set Cartesian axes x and y defined by $R_{yx} = R_y R_x$ or $R_{xy} = R_x R_y$. These have the general form

$$
\begin{aligned}
R_{yx} &= \begin{pmatrix} \cos\phi_y & -\sin\phi_x \sin\phi_y & \cos\phi_x \sin\phi_y \\ 0 & \cos\phi_x & \sin\phi_x \\ -\sin\phi_y & -\sin\phi_x \cos\phi_y & \cos\phi_x \cos\phi_y \end{pmatrix}, \\
R_{xy} &= \begin{pmatrix} \cos\phi_y{}' & 0 & \sin\phi_y{}' \\ -\sin\phi_x{}' \sin\phi_y{}' & \cos\phi_x{}' & \sin\phi_x{}' \cos\phi_y{}' \\ -\cos\phi_x{}' \sin\phi_y{}' & -\sin\phi_x{}' & \cos\phi_x{}' \cos\phi_y{}' \end{pmatrix},
\end{aligned} \tag{4}
$$

and both converge to the above operator (3) in the small angle approximation. On the other hand, they represent intrinsically different operators for large angles[1].

Indeed, the two angular data extracted from the direction of $\hat{m}$ are not sufficient to determine uniquely the 3-DoF configuration, and the selection of a particular rotation order corresponds to arbitrarily assign the missing information. Such an approach allows for producing tentative eye gaze trajectories, but the solution is not stringent and diverse choices results in diverse and variously distorted trajectories. Nevertheless, also with this under-specified analysis, the main features of the gaze trajectories can be identified, which can be satisfactory in some eye-tracking applications.

As an example, in Fig.2 we represent tracking results obtained in a in-vivo experiment, using the R_{xy} and R_{yx} operators alternatively. The subject was requested to read a short text (title, a complete line, a half-line) on a monitor and then to follow the monitor frame. The four represented trajectories are obtained from the same dataset, with an analysis of the dipole orientation based upon the two operators, respectively. In this elaboration, one selects (tentatively) the $\hat{m}_0$ orientation, i.e. the trajectory point to which the $(\phi_x = 0, \phi_y = 0)$ co-ordinates are being assigned in such a way to obtain as straight lines and right angles as possible. As one can see, in all cases features like text line distribution and small displacements around the running line of sight are well tracked, while distortions can't be canceled and affect long segments that should be straight and angles at the monitor corners that should be right.

The subject was sitting in front of the monitor so that $\hat{e}_0$ is expected to coincide with (to be in the proximity of) the measurement tracked at the monitor center. Two of the trajectories –(a) and (c)– are obtained in this hypothesis, assigning $\hat{e}_0$ to the central point of the figure (thus selecting the corresponding $\hat{m}$ as $\hat{m}_0$). The other trajectories –(b) and (d)– are instead obtained with a wrong assignment ($\hat{e}_0$ in coincidence of the upper-left corner, about 20 degree away from the nominal direction). As can be seen, the main features of the trajectory are well reproduced also in this case, which demonstrates robustness with respect to the $(\hat{e}_0, \hat{m}_0)$ assignment.

Is worth reminding that in principle, also the $\hat{e}_0$ could be at some angle from $\hat{z}$, however this angle amounts at less then $10°$ and it would cause minor changes to the plots shown in Fig.2.

---

[1] Indeed the two operators coincide if $\phi_x = \phi_x{}' = 0$ or $\phi_y = \phi_y{}' = 0$, that is if one of the two x or y axes happens to be the unique rotation axis. This has a practical utility that will be discussed in subsection 3.3
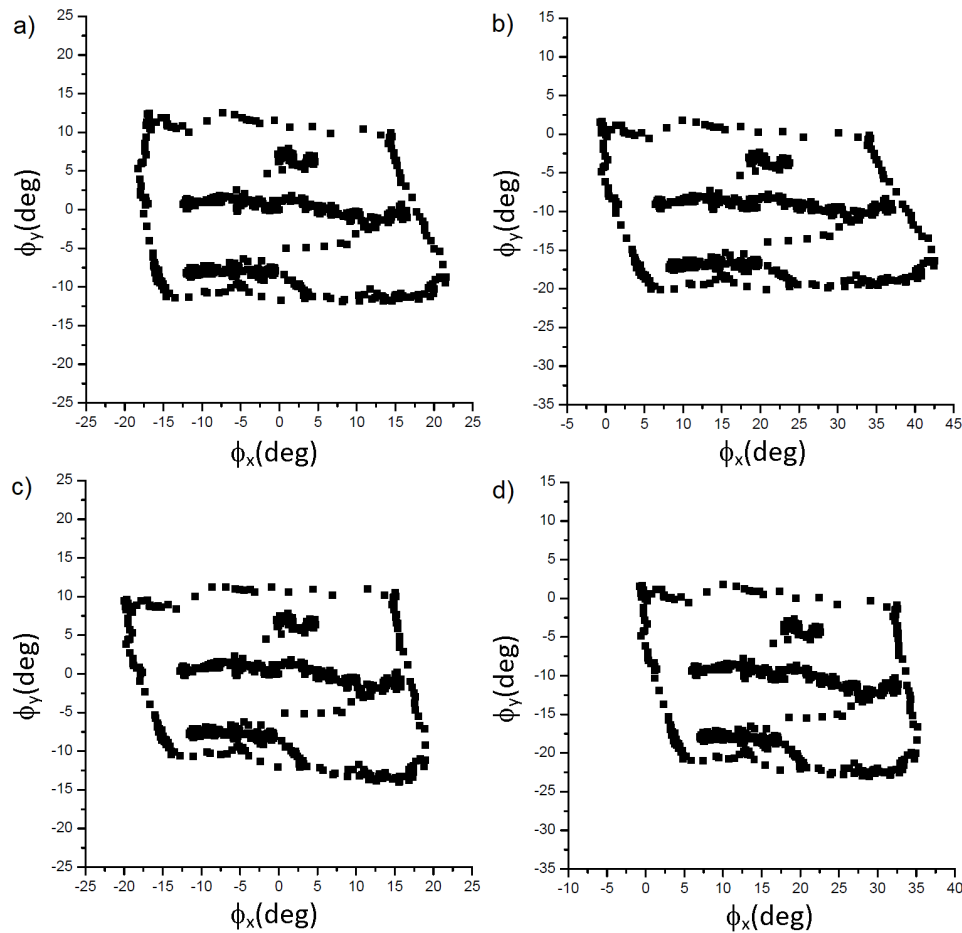
Figure 2. Gaze trajectories reconstructed on the basis of the approach described in Sec.3.2. The subject was sitting about 110 cm away from a monitor, whose frame is 40 cm × 71.5 cm in size. He was requested to read a three-line text and then to follow the monitor frame (see also Fig.5). The upper plots (a,b) are obtained using $R = R_y R_x$, while the lower ones (c, d) are obtained with $R = R_x R_y$. The front sight direction (0,0) is not known and is in turn assigned to a central point of the screen (left plots, a, c), or to the upper-left corner (right plots, b, d). The small displacements of the trajectory are well tracked in all the cases, but evident image distortions occur over the large distances, i.e. when large rotations are involved. This kind of distortion arises independently on the assignment of the front-sight direction.

3.3. Large rotations about an assigned axis

The issue related to the non commutativity of finite 3D rotation is overcome in a preeminent application of the eye-tracking systems. In VOR measurements, the head of the patient is rotated around a predetermined axis, which is usually vertical (pitch) or horizontal (yaw), the expected (ideal) response of the eye is an opposite (compensating) rotation around the same axis, and this is the quantity to be estimated and analyzed.

In this case, the data are to be interpreted in terms of a single rotation angle around one axis. That axis can be assumed to coincide with the nominal one that is *approximately* either the $\hat{x}$ or the $\hat{y}$ direction defined in Fig.1 in the cases of pitch or yaw, respectively.

Improved accuracy is achieved if the actual rotation axis is identified on the basis of the $\vec{B}_{geo}$ measurement set $\{\vec{B}_i\}$ $(i = 1, \ldots, N)$ recorded during the maneuver. For instance, one can find the common plane intercepting the measured $\vec{B}_i$ vectors (with a mean square distance minimization). The perpendicular direction to the plane, $\hat{u}$, provides an estimate of the rotation axis direction [23,24].

Subsequently, both the head and eye rotations can be evaluated around the determined direction. The eye rotation angle can be estimated from two measured values $\vec{m}_i$ ($i = 1, 2$) as

$$\phi_{u,1} - \phi_{u,2} = \arcsin \frac{|\vec{m}_{1,\perp} \times \vec{m}_{2,\perp}|}{|m_{1,\perp}||m_{2,\perp}|} \tag{5}$$

182 being $\vec{m}_{i,\perp} = \vec{m}_i - (\vec{m}_i \cdot \hat{u})\hat{u}$, and similarly –using $\vec{B}_{geo}$– for the head.

183   This perfecting produces just a slight enhancement of the accuracy, if the misalignment between
184 ideal and actual rotation axes is small, i.e. $\hat{u} \approx \hat{x}$ or $\hat{u} \approx \hat{y}$. Whatever the actual rotation axis is, in
185 this application eye and head rotations never exceed $\pi/2$, which makes unnecessary to refine eq.5 for
186 out-of-range arcsine issues.

187   An alternative method to determine the rotation axis is fitting a 3D circle on the $\vec{B}_i$, as $\vec{B}$ moves
188 nominally on a circle at constant zenithal angle with respect to the rotation axis [25]. To this end, we
189 have implemented a procedure that:

190   • applies a rotation matrix parametrized with a couple of Euler angles (α, β) to a set $\{\vec{B}_i\}$ or $\{\vec{m}_i\}$;
191   • represents the data in spherical co-ordinates;
192   • determines the couple (α, β) as that minimizing the standard deviation of the zenithal angles.

193   Considering the case of a generic rotation, it is worth noting that the VOR gain is not isotropic
194 [26,27], so that –also in the simplified assumption of a linear and non-delayed response– the VOR gain
195 should be expressed tensorially. E.g., focusing on the angular velocities, the relationship between eye
196 and head speed would be expressed as $\vec{\omega}_e = G\vec{\omega}_h$, where G is a 3×3 matrix. G is expected to be a
197 non-diagonal matrix, implying that eye and head rotation axes are generally not parallel. A correct and
198 complete analysis of the VOR gain involves the determination of all the elements G_{ij}, which (at least in
199 principle) can be obtained from the above described data. The way this task should be accomplished
200 goes beyond of the scopes of this paper.

201   As an additional remark, is worth noting that our prototype contains only magnetometric sensors,
202 however improved setups could be designed to include gyroscopic detectors. In this case, additional and
203 complementary estimates of the head rotations would be available, with improved accuracy in VOR
204 gain estimations.
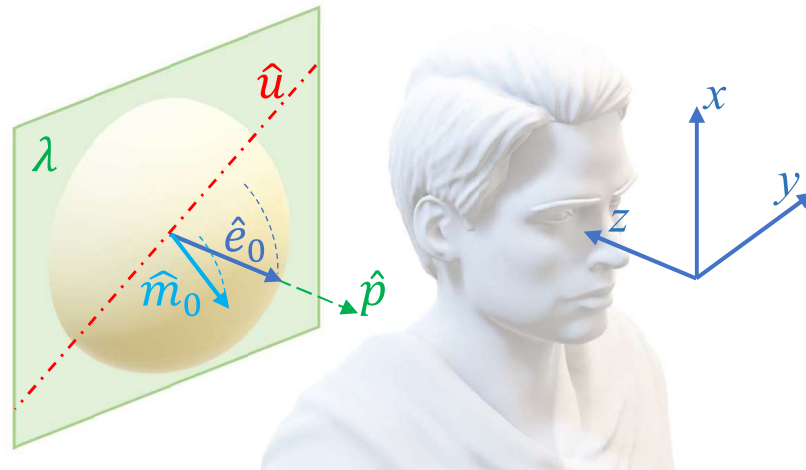
3.4. Physiological constraints

Figure 3. Definition of the axes and geometry of the Listing's model. The primary orientation $\hat{e}_0$ (along the normal $\hat{p}$ to the Listing's plane λ) is nearly parallel to $\hat{z}$. In our setup, when the eye is in its primary orientation the magnetic dipole is generically oriented ($\hat{m}_0$). When the gaze varies, both vectors $\vec{m}$ and $\hat{e}$ undergo rotations (dashed arcs) obeying the Listing's law: each accessible configuration is such that it could be reached from the primary orientation with one rotation around an axis laying on λ. In this figure, the direction $\hat{u}$ embodies one of those axes.

The arbitrariness of the rotation matrix introduced in Sec.3.2 (eq.4) can be avoided if the DoF reduction is performed on the basis of physiological constraints of the eye. Torsional movements of the eye are strongly depressed and in a good approximation the eye movements respect a 1D constraint enunciated in the 19th century and named Donders' law. Abundant literature is available on this subject. The reader may find a useful introduction to the matter in Ref.[28] and more mathematical details in Ref.[29]. Donders' law states that each direction of the gaze corresponds to a single orientation of the eye, regardless of the trajectory that led to the corresponding eye pose. In other words, each direction of view corresponds to a unique eye configuration and torsional movements around the current line of sight do not occur or can be neglected.

As far as the Donders' law is respected, the eye movements have only two DoF, hence it is possible to search for a biunique relationship between $\hat{m}$ and $\hat{e}$. A second phenomenological law that rules the eye movement is known as Listing's law. It suggests a good parametrization to describe these two-DoF configurations allowed by the Donders' law.

According to the Listing's law, there exists a direction (primary orientation) ($\hat{p}$) such that any eye configuration can be described as if reached moving from that primary orientation by means of a single rotation around an axis perpendicular to $\hat{p}$, as sketched in Fig.3.

In other terms, making reference to a spherical co-ordinate systems having the polar axis along $\hat{p}$, all the eye configurations can be reached with one opportune zenithal rotation from the primary orientation: the rotation axes lay on the equatorial plane of that co-ordinate system, the so-called Listing's plane. When the head is erect and the eye is at the primary orientation, the gaze is approximately straight ahead, thus the Listing's plane is not far from being vertical.

Summarizing, the Listing's law reduces the DoF of eye configuration to two: each eye configuration can be considered as the result of a rotation by a given zenithal angle around an axis $\hat{u}$ that lays on the Listing's plane and has a given orientation (azimuthal angle) on that plane. The data elaboration needed to retrieve $\hat{e}_i$ from $\hat{m}_i$ consists in the determination of those two angles from the current orientation of

231 the dipole ($\hat{m}_i$) and its orientation ($\hat{m}_0$) when the gaze is along the primary direction. This problem is
232 focused in next Sec. 3.5.

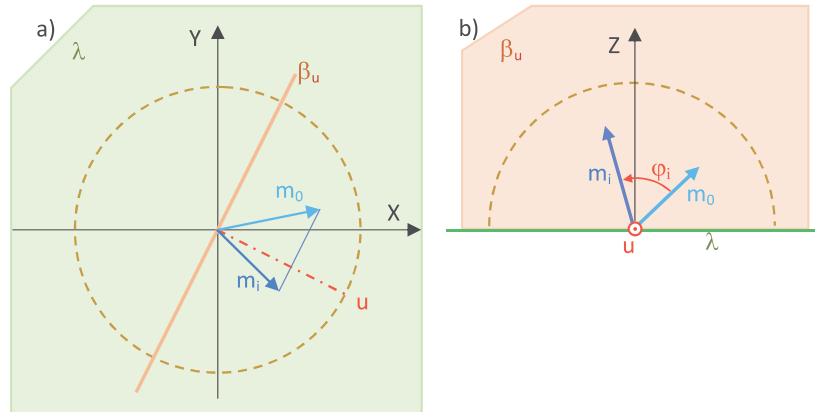233 *3.5. Applying the Listing's law to the present case*

Figure 4. In the rotated system XYZ, the Listing's plane λ is the XY plane. In (a) the projections
of $\hat{m}_0$ and $\hat{m}_i$ on that plane are represented. The rotation axis $\hat{u}$ lays on that plane and is identified
as the normal to the difference between the projections of $\hat{m}_0$ and $\hat{m}_i$. The direction of $\hat{u}$, together
with the Z axis, identifies the plane β_u. In (b) the projections of $\hat{m}_0$ and $\hat{m}_i$ on β_u are shown: β_u is
the plane where the rotation angle φ_i around $\hat{u}$ can be evaluated.

234 In our implementation, $\hat{p}$ is approximately antiparallel to $\hat{z}$. Let $\hat{p}$ be known or tentatively assigned
235 (see below). First of all we refer the tracking data to a rotated coordinate system XYZ such that
236 $\hat{p} = -\hat{Z}$. To this end, we determine the Rodrigues' matrix [30,31] that leads $\hat{z}$ to coincide with $\hat{Z} = -\hat{p}$
237 and we use this matrix to represent the measurements $\vec{m}_i$ in these new co-ordinates XYZ, where the
238 Listing's plane is the XY plane[2].
239 Let $\hat{m}_0$ and $\hat{e}_0$ be the magnet and the eye directions corresponding to the primary orientation: by
240 definition, $\hat{e}_0 = -\hat{Z}$, while $\hat{m}_0$ must be known or tentatively assigned. The task is now to determine the
241 orientation $\hat{e}_i$ corresponding to the measured $\hat{m}_i$ on the basis that $\hat{e}_i = R_{\varphi_i,\hat{u}_i}\hat{e}_0$ and $\hat{m}_i = R_{\varphi_i,\hat{u}_i}\hat{m}_0$,
242 where $R_{\varphi_i,\hat{u}_i}$ is a rotation by an angle θ around the direction $\hat{u}$ that lies on the XY plane (again, the
243 Rodrigues' formula can be used to determine the corresponding matrix).
244 $R_{\varphi_i,\hat{u}_i}$ can be uniquely determined from $\hat{m}_0$ $\hat{m}_i$ as follows. The rotation axis $\hat{u} = (u_X, u_Y, 0)$ is
245 perpendicular to the projection of $\Delta\hat{m} = \hat{m}_0 - \hat{m}_i$ on the XY plane: $\hat{u} \cdot (m_{0X} - m_{iX}, m_{0Y} - m_{iY}, 0) = 0$.
246 Now consider the projections of $\hat{m}_0$ and $\hat{m}_i$ on the plane perpendicular to $\hat{u}$: φ_i the angle between
247 those projections can be evaluated with the method described by eq.5. The retrieved $\hat{u}$ and ϕ_i give the
248 axis and the rotation angle, respectively, in the Listing's model of the eye.
249 When $\hat{p}$ and/or $\hat{m}_0$ are not known *a priori*, they can be tentatively assigned and their
250 appropriateness can be evaluated on the basis of the distortion of the reconstructed gaze trajectory
251 corresponding to regular and known shapes. This is the case of the trajectory represented in Fig.5.
252 The same recording used for Fig.2 is here processed according to the above described Listing's model
253 procedure. A direct comparison with the trajectories shown in Fig.2 puts in evidence a clear reduction of

---

[2]   Note that the reference axis X can be arbitrarily chosen on the Listing's plane, since all data of interest are related to
angular displacements (and not to absolute directions).

distortion effects. On the basis of this observation, we conclude that the Listing's law makes it possible
to develop a good procedure to accurately retrieve the eye-gaze, despite the $\hat{m} - \hat{e}$ misalignment.
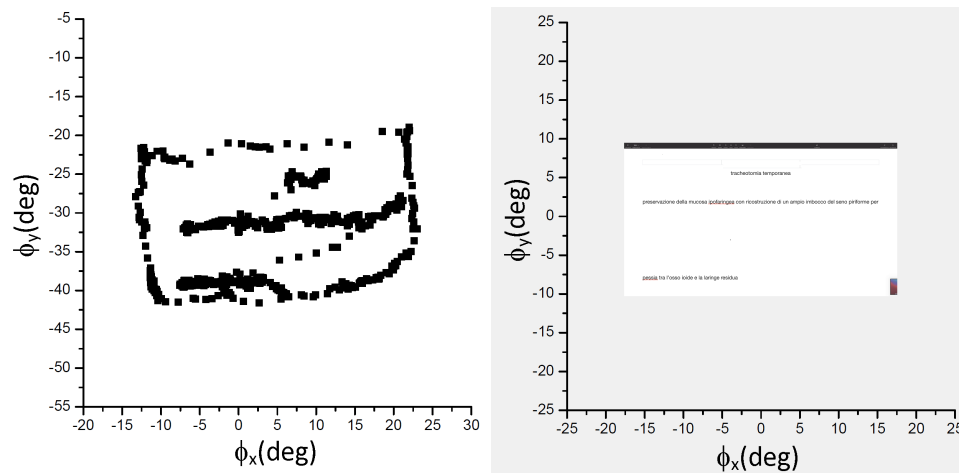

Figure 5. The same data used to produce the gaze trajectories represented in Fig. 2 are here
elaborated on the basis of the Listing's model. With an appropriate selection of the $\hat{m}_0$ and $\hat{p}$
directions, the whole data set fits with much lower distortion onto a shape that reproduces the text
and the monitor frame observed by the subject (sketched in the right figure).

A *hardware* solution based on an accurate alignment of the magnetic dipole with the lens optical
axis would greatly simplify the task of retrieving the gaze from the measured $\hat{m}$. To this aim, the
magnetic disc should be inserted out of the lens axis (to be non obstructive for the view) and tilted
with respect to the lens surface, which comes with some geometrical issues, as sketched in Fig.6 b,c.
In the scheme 6 b, for instance, $\hat{e}_0$ and $\hat{m}_0$ come to a complete identity and no reciprocal rotation
has to be measured or estimated. The scheme 6 c, instead, opens new possibilities by allowing direct
measurements of the torsional movement of the eye. These interesting perspectives are beyond the
scope of the present work and will be subject of further investigation.

3.6. Retrieving the eye gaze from the magnet position

An alternative approach that could enable the estimation of the eye orientation with respect to the
sensor array is based on the analysis of the magnet position. As said (Sec.2.2), the best fit procedure
provides, beside $\vec{B}_{geo}$ and $\vec{m}$, also the position $\vec{r}$ of the dipole. As far as the eye is adequately described
in terms of a fixed-centre sphere, $\vec{r}$ is expected to move on a spherical surface. The radius of that sphere
is the eye radius (12 mm, as a typical value), and its center is located at the eye center $\vec{R}_e$, which is (at
least initially) an unknown position.

In principle (see Fig.7), one could first determine $\vec{R}_e$ fitting a large set of $\{\vec{r}_i\}$ on a sphere and
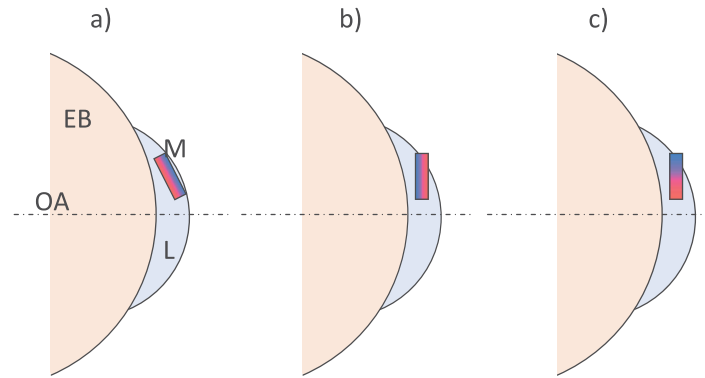then use the quantities $\{\vec{s}_i = \vec{r}_i - \vec{R}_e\}$, similarly to what is done with $\vec{m}$.

Figure 6. Schematic representation (not to scale) of an eye-ball (EB) (OA is its optical axis) wearing a lens (L) with a magnetized disk (M) embedded. The red-blue colors represent the M magnetization. In the current implementation (a), the disk is axially magnetized and is inserted tangentially to the lens, a few mm displaced from the optical axis. This reduces the magnet encumbrance, at expenses of a $\hat{m} - \hat{e}$ misalignment and consequent need of indirect gaze retrieval. Constructive efforts can be devoted to make the dipole parallel to the gaze direction (b) or perpendicular to it (c). This would simplify the data elaboration and –in the case (c), i.e. with a diametrical magnetization– it would make the system highly responsive to torsional movements: an unprecedented feature of this methodology. As sketched, the (b) and (c) arrangements may present issues to guarantee a complete magnet embedding)
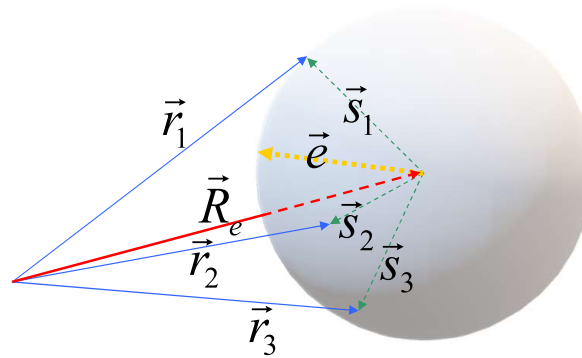

Figure 7. The retrieved positions $\vec{r}_i$ are determined with respect to the sensor array frame. A large set $\vec{r}_i$ might enable the determination of the eye center $\vec{R}_e$, and hence the positions $\vec{s}_i$ with respect to the eye center. The gaze orientation $\vec{e}$ moves rigidly with the position $\vec{s}$ of the magnet, and $\vec{s}$ could be used alternatively to (or in conjunction with) $\vec{m}$ to determine $\vec{e}$. This requires that $\vec{R}_e$ is determined with a high accuracy, which is not the case due to the small range of available $\vec{r}_i$.

More interestingly, provided that $\hat{m}$ e $\hat{s}$ are not parallel, it would be possible to use both to determine the eye orientation with no need for extra hypotheses. Indeed, $\hat{m}$, $\hat{s}$ (e.g. together with $\hat{m} \times \hat{s}$) would constitute a basis in the 3D space, hence the matrix R such that $\hat{m}_i = R\hat{m}_0$ and $\hat{s}_i = R\hat{s}_0$ would be uniquely determined (even over-determined) from two subsequent estimates of $\hat{m}$ and $\hat{s}$.

Physiological constraints prevent $\vec{r}$ from ranging over a sufficiently wide portion of the spherical surface and this results in a rather rough estimation of $\vec{R}_e$. As a consequence, these alternative approaches –at least with the precision achieved in current implementation– do not help improve the quality of the gaze estimations.

4. Conclusion

An innovative eye-tracker is developed, based on non-inductive magnetometric measurements simultaneously performed at 100 Sa/s rate in a set of prearranged positions with the aid of an array of magnetoresistive sensors. This kind of instrumentation extends to the eye-tracking some advantageous features of similar magnetostatic trackers developed for other applications.

Moderate invasivity, high speed, spatial and angular accuracy, robustness, simplicity and low cost emerge as attractive characteristics in comparison with other eye-tracking technologies.

Despite position and orientation of the magnet are fully characterized, the conversion of magnet tracking data to gaze information is not immediate and may require specific procedures. In this paper, we have examined the problem of retrieving the eye gaze from the magnet orientation when eye and dipole are not parallel.

In particular, we have demonstrated how the combination of tracking parameters with physiological constraints of the eye motion enables an accurate reconstruction of the eye-gaze trajectories, while alternative simplified analyses can be implemented and –despite some distortion effects– they enable the extraction of basic features of the gaze trajectory.

5. Acknowledgments

Patents A patent [32] is pending about inventions related to this research.

Data Availability Statement: The datasets generated and analyzed during the current study are available from the corresponding author on reasonable request.

Informed Consent Statement: Informed consent was obtained from all subjects involved in the study. In particular, the system was worn by a scientist who actively participates in these studies and in this research.

Author Contributions: Conceptualization, V.B., P.C..; Data curation, V.B.; Formal analysis, V.B, P.C.; Funding acquisition, V.B.; Investigation, V.B., P.C.; Methodology, V.B., P.C.; Project administration, V.B.; Resources, V.B.; Software, V.B.; Supervision, V.B.; Validation, V.B., P.C.; Visualization, V.B.; Writing—original draft, V.B.; Writing—review & editing, V.B., P.C. All authors have read and agreed to the published version of the manuscript.

Conflicts of Interest: Authors declare that they have applied for the above mentioned patent [32]. This the only potential conflict of interest.

1. Than, T.D.; Alici, G.; Zhou, H.; Li, W. A Review of Localization Systems for Robotic Endoscopic Capsules. *IEEE Transactions on Biomedical Engineering* **2012**, *59*, 2387–2399. doi:10.1109/TBME.2012.2201715.
2. Di Natali, C.; Beccani, M.; Valdastri, P. Real-Time Pose Detection for Magnetic Medical Devices. *IEEE Transactions on Magnetics* **2013**, *49*, 3524–3527. doi:10.1109/TMAG.2013.2240899.
3. Jucevičius, M.; Ožiūnas, R.; Narvydas, G.; Jegelevičius, D. Permanent Magnet Tracking Method Resistant to Background Magnetic Field for Assessing Jaw Movement in Wearable Devices. *Sensors* **2022**, *22*. doi:10.3390/s22030971.
4. Kolder H, E. Electro-Oculography. *Ophthalmologica* **1974**, pp. 127–140. doi:10.1159/000307117.
5. Kumar, A.; Krol, G. Binocular infrared oculography. *Laryngoscope* **1992**, pp. 367–378. doi:10.1288/00005537-199204000-00002.

6.   Aungsakun, S.; Phinyomark, A.; Phukpattaranont, P.; Limsakul, C. Development of robust electrooculography (EOG)-based human-computer interface controlled by eight-directional eye movements. *International journal of physical sciences* **2012**, *7*, 2196–2208.

7.   Kimmel, D.; Mammo, D.; Newsome, W. Tracking the eye non-invasively: simultaneous comparison of the scleral search coil and optical tracking techniques in the macaque monkey. *Frontiers in Behavioral Neuroscience* **2012**, *6*, 49. doi:10.3389/fnbeh.2012.00049.

8.   Houben, M.M.; Goumans, J.; van der Steen Johannes. Recording three-dimensional eye movements: scleral search coils versus video oculography. *Invest Ophthalmol Vis Sci.* **2006**, *47*, 179–187. doi:10.1167/iovs.05-0234.

9.   Robinson, D.A. A Method of Measuring Eye Movemnent Using a Scleral Search Coil in a Magnetic Field. *IEEE Transactions on Bio-medical Electronics* **1963**, *10*, 137–145. doi:10.1109/TBMEL.1963.4322822.

10. Collewijn, H.; van der Mark, F.; Jansen, T. Precise recording of human eye movements. *Vision Research* **1975**, *15*, 447–IN5. doi:https://doi.org/10.1016/0042-6989(75)90098-X.

11. Agrawal, Y.; Schubert, M.C.; Migliaccio, A.A.; Zee, D.S.; Schneider, E.; Lehnen, N.; Carey, J.P. Evaluation of quantitative head impulse testing using search coils versus video-oculography in older individuals. *Otol Neurotol.* **2014**, *35*, 283–288. doi:10.1097/MAO.0b013e3182995227.

12. Otero-Millan, J.; Roberts, D.C.; Lasker, A.; Zee, D.S.; Kheradmand, A. Knowing what the brain is seeing in three dimensions: A novel, noninvasive, sensitive, accurate, and low-noise technique for measuring ocular torsion. *Journal of Vision* **2015**, *15*, 11–11, [https://arvojournals.org/arvo/content_public/journal/jov/934563/i1534-7362-15-14-11.pdf]. doi:10.1167/15.14.11.

13. Tarantino, S.; Clemente, F.; De Simone, A.; Cipriani, C. Feasibility of Tracking Multiple Implanted Magnets With a Myokinetic Control Interface: Simulation and Experimental Evidence Based on the Point Dipole Model. *IEEE Transactions on Biomedical Engineering* **2020**, *67*, 1282–1292. doi:10.1109/TBME.2019.2935229.

14. Gherardini, M.; Mannini, A.; Cipriani, C. Optimal Spatial Sensor Design for Magnetic Tracking in a Myokinetic Control Interface. *Computer Methods and Programs in Biomedicine* **2021**, *211*, 106407. doi:https://doi.org/10.1016/j.cmpb.2021.106407.

15. Ge, H.; Song, S.; Wang, J.; Meng, M.Q.H. Multi-Magnet Tracking Method using Extended Kalman Filter. 2021 IEEE Sensors, 2021, pp. 1–4. doi:10.1109/SENSORS47087.2021.9639620.

16. Jaufenthaler, A.; Schier, P.; Middelmann, T.; Liebl, M.; Wiekhorst, F.; Baumgarten, D. Quantitative 2D Magnetorelaxometry Imaging of Magnetic Nanoparticles Using Optically Pumped Magnetometers. *Sensors* **2020**, *20*. doi:10.3390/s20030753.

17. Tanwear, A.; Liang, X.; Liu, Y.; Vuckovic, A.; Ghannam, R.; Böhnert, T.; Paz, E.; Freitas, P.P.; Ferreira, R.; Heidari, H. Spintronic Sensors Based on Magnetic Tunnel Junctions for Wireless Eye Movement Gesture Control. *IEEE Transactions on Biomedical Circuits and Systems* **2020**, *14*, 1299–1310. doi:10.1109/TBCAS.2020.3027242.

18. Biancalana, V.; Cecchi, R.; Chessa, P.; Bevilacqua, G.; Dancheva, Y.; Vigilante, A. Fast, Cheap, and Scalable Magnetic Tracker with an Array of Magnetoresistors. *Instruments* **2021**, *5*. doi:10.3390/instruments5010003.

19. iSentek. *IST 8308 - 3D Magnetometer - Brief datasheet*, 2017. Rev. 1.0 available at http://www.isentek.com/en/dlf.php?file=../ISENTEK/(201703-20)IST8308Datasheetv1.0_brief.pdf.

20. Biancalana, V.; Cecchi, R.; Chessa, P.; Mandalà, M.; Bevilacqua, G.; Dancheva, Y.; Vigilante, A. Validation of a Fast and Accurate Magnetic Tracker Operating in the Environmental Field. *Instruments* **2021**, *5*. doi:10.3390/instruments5010011.

21. Bellizzi, L.; Bevilacqua, G.; Biancalana, V.; Carucci, M.; Cecchi, R.; Chessa, P.; Donniacuo, A.; Mandalà, M.; Stiaccini, L. An innovative eye-tracker: Main features and demonstrative tests. *Review of Scientific Instruments* **2022**, *93*, 035006, [https://doi.org/10.1063/5.0079779]. doi:10.1063/5.0079779.

22. Crawford, J.D.; Vilis, T. Axes of eye rotation and Listing's law during rotations of the head. *Journal of Neurophysiology* **1991**, *65*, 407–423, [https://doi.org/10.1152/jn.1991.65.3.407]. PMID: 2051188, doi:10.1152/jn.1991.65.3.407.

23. Pearson, K. On lines and planes of closest fit to systems of points in space. *The London, Edinburgh, and Dublin Philosophical Magazine and Journal of Science* **1901**, *2*, 559–572, [https://doi.org/10.1080/14786440109462720]. doi:10.1080/14786440109462720.

24. Schomaker, V.; Waser, J.; Marsh, R.E.; Bergman, G. To fit a plane or a line to a set of points by least squares. *Acta Crystallographica* **1959**, *12*, 600–604. doi:10.1107/S0365110X59001748.

25. Fisher, B. Least-square fitting of circles to 3D point data. https://homepages.inf.ed.ac.uk/rbf/CVonline/LOCAL_COPIES/FISHER/CIRCLEFIT/fit3dcircle/fit3dcircle.html, 2017.

26. Aw, S.T.; Halmagyi, G.M.; Haslwanter, T.; Curthoys, I.S.; Yavor, R.A.; Todd, M.J. Three-dimensional vector analysis of the human vestibuloocular reflex in response to high-acceleration head rotations. II. responses in subjects with unilateral vestibular loss and selective semicircular canal occlusion. *Journal of Neurophysiology* **1996**, *76*, 4021–4030, [https://doi.org/10.1152/jn.1996.76.6.4021]. PMID: 8985897, doi:10.1152/jn.1996.76.6.4021.

27. Pogson, J.M.; Taylor, R.L.; Bradshaw, A.P.; McGarvie, L.; D'Souza, M.; Halmagyi, G.M.; Welgampola, M.S. The human vestibulo-ocular reflex and saccades: normal subjects and the effect of age. *Journal of Neurophysiology* **2019**, *122*, 336–349, [https://doi.org/10.1152/jn.00847.2018]. PMID: 31042447, doi:10.1152/jn.00847.2018.

28. Wong, A.M. Listing's law: clinical significance and implications for neural control. *Survey of Ophthalmology* **2004**, *49*, 563–575. doi:https://doi.org/10.1016/j.survophthal.2004.08.002.

29. Haslwanter, T. Mathematics of three-dimensional eye rotations. *Vision Research* **1995**, *35*, 1727–1739. doi:https://doi.org/10.1016/0042-6989(94)00257-M.

30. Rodrigues, B.O. Des lois géométriques qui régissent les déplacements d'un système solide dans l'espace, et de la variation des coordonnées provenant de ces déplacements considérés indépendamment des causes qui peuvent les produire" (On the geometrical laws that govern the displacements of a solid system in space, and on the change of coordinates resulting from these displacements considered independently of the causes that can produce them). *Journal de Mathématiques Pures et Appliquées* **1840**, *5*, 380–440.

31. Cheng, H.; Gupta, K.C. An Historical Note on Finite Rotations. *Journal of Applied Mechanics* **1989**, *56*, 139–145, [https://asmedigitalcollection.asme.org/ appliedmechanics/ article-pdf/56/1/139/5460585/139_1.pdf]. doi:10.1115/1.3176034.

32. Biancalana, V.; Cecchi, R.; Chessa, P.; Mandalà, M.; Prattichizzo, D. Patent pending: System for tracking an object, 2020. 102020000017776 July 22nd 2020; PCT WO2022/018691-A1 Jan 27th 2022.